

A Case for Quantum Circuit Cutting for NISQ Applications: Impact of topology, determinism, and sparsity

Zirui Li
zirui.li@rutgers.edu
Rutgers University
USA

Minghao Guo
mg1998@scarletmail.rutgers.edu
Rutgers University
USA

Mayank Barad
mb1961@scarletmail.rutgers.edu
Rutgers University
USA

Wei Tang
weit@alumni.princeton.edu
Princeton University
USA

Eddy Z. Zhang
eddy.zhengzhang@gmail.com
Rutgers University
USA

Yipeng Huang
yipeng.huang@rutgers.edu
Rutgers University
USA

Abstract

We make the case that variational algorithm ansatzes for near-term quantum computing are well-suited for the quantum circuit cutting strategy. Previous demonstrations of circuit cutting focused on the exponential execution and post-processing costs due to the cuts needed to partition a circuit topology, leading to overly pessimistic evaluations of the approach. This work observes that the ansatz Clifford structure and variational parameter pruning significantly reduce these costs. By keeping track of the limited set of correct subcircuit initializations and measurements, we reduce the number of experiments needed by up to $16\times$, matching and beating the error mitigation offered by classical shadows tomography. By performing reconstruction as a sparse tensor contraction, we scale the feasible ansatzes to over 200 qubits with six ansatz layers, beyond the capability of prior work.

1 Introduction

There is significant excitement about when quantum computing might first become useful [20]. The first applications of QC are expected to be in the simulation of quantum systems [27]. Furthermore, it is expected that any early applications of QC will require tight cooperation between classical and quantum computing. Although proposals of hybrid quantum-classical computing seem pragmatic, exactly how the two computing paradigms might interact is an open question. The ways in which problems, algorithms, and solution data are represented in QC and classical computing are vastly different and do not allow for tight coupling [36, 46, 49].

One straightforward strategy is to phrase problems and algorithms entirely in the QC paradigm and allow classical computing to augment the capability of QCs [53]. In such an approach, quantum programs, known as quantum circuits, are carefully split apart such that the program fragments run independently. The fragments are expected to perform with greater success in QCs due to their lower hardware requirements, shorter execution duration, and easier compilation of the problems in terms of hardware constraints. A classical computer gathers the data collected from the individual QC experiments and reconstructs the complete

result [9, 34, 50, 58–60]. The interaction of classical and quantum hardware and software leads to architectural questions.

The strategy has significant momentum. Various research studies have investigated the most beneficial way to decompose circuits to fit in constraints [9, 34, 50, 59, 60], along with the most efficient way to perform experiment measurements that collect data for classical reconstruction [14–16]. Industrial strength libraries for planning reconstruction computation [26] and for performing actual reconstruction on GPUs [3] all highlight the expectation that the strategy will have a practical impact.

The strategy also has critics. It is understood that the number of cuts that are used to split the quantum programs—the *topology* of a quantum circuit and its partitioning [6, 44]—dictates the both the cost of subcircuit executions and the cost of reconstruction classical postprocessing.

This paper considers these costs by exploiting orthogonal and previously overlooked opportunities.

First, in quantum algorithms where a quantum circuit is run repeatedly with different parameters [22, 54], a lot of information can be gathered once the circuit topology and cutting plan are established. In fact, the states to which subcircuits must be initialized and measured are already known *deterministically* at this point. The challenge in exploiting this knowledge is how to collect, compile, and query this information efficiently to drive the circuit cutting strategy. In this work, we address this challenge using established techniques in classical artificial intelligence to reason about deterministic information in otherwise probabilistic models [19]. We apply these techniques to efficiently perform circuit cutting experiments with minimal sets of initializations and measurements, thus reducing the number of experiments needed to reach a given level of precision by $16\times$. The compiled knowledge furthermore creates an opportunity to reduce error in the reconstructed result, thus matching or beating existing error mitigation approaches in quantum state tomography.

Second, because of the structure and determinism in the data collected from the quantum subcircuit executions, the measurement data are extremely *sparse*. Specifically, of the

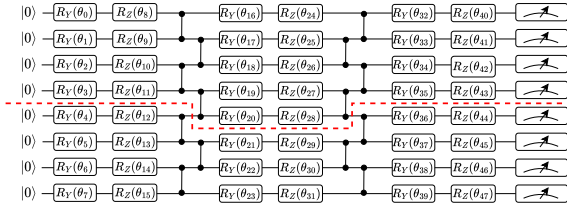


Figure 1. The circuit cutting plan for HWEA with #qubits 8, depth 2. The qubit constraint for each subcircuit is 5. We use HWEA (8,2,5) to describe this circuit cutting workload.

possible initializations and measurement outcomes that are possible, only very few sets have coefficients that contribute to the reconstructed state. In practice, this means that previous approaches to performing reconstruction as conventional tensor multiplication have had significantly inflated and conservative cost estimates. For nontrivial circuits, we demonstrate a reduction in memory required by more than 90%, and we expand the size of ansatzes that are feasible in the circuit strategy to over 200 qubits, surpassing prior work.

2 Motivation & Background

Current quantum computer prototypes are limited in both capacity and accuracy. Researchers believe that the first applications of noisy intermediate-scale quantum (NISQ) computing would be through variational quantum algorithms (VQAs) [48, 55]. This section reviews existing work on VQAs, focusing on how they are especially suited for the quantum circuit cutting strategy. Then, we review the necessary mathematical background for VQAs and circuit cutting.

2.1 Motivation for NISQ Circuit Cutting

A major concern about quantum circuit cutting is the exponential costs in quantum circuit executions and classical post-processing. Due to these concerns, some types of quantum circuit have been found to be non-scalable in the circuit cutting strategy [50]. This paper makes a case that quantum circuits for NISQ era VQAs have favorable properties in terms of topology, determinism, and sparsity such that they work well with circuit cutting.

VQAs overcome limitations in the accuracy and capacity of QC by combining the strengths of quantum computers and classical optimization. The quantum circuits serve to evaluate a high-dimensional objective function parameterized by rotation angles. A classical optimizer drives the QC executions, tuning the rotation angles to minimize the objective function. VQAs span the full range of envisioned near-term applications of QCs, including quantum chemistry [13, 33, 42, 45, 54], optimization [22, 32], and machine learning classification [61].

It has been observed that VQA ansatz circuits have topologies that are suitable for circuit cutting. In previous studies,

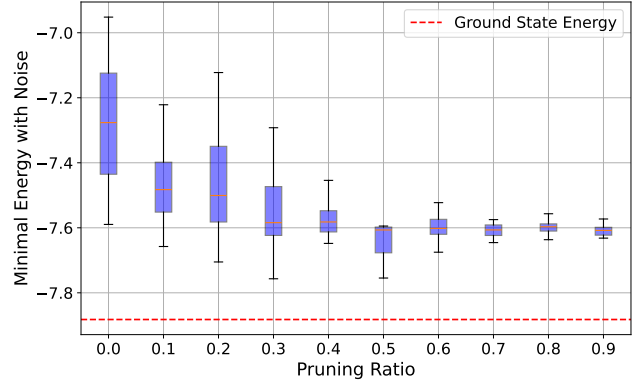


Figure 2. Pruning non-Clifford gates with small rotation angles is an effective strategy for NISQ ansatzes. The plot shows the calculated ground state energy from the ansatz for progressively larger pruning ratios. The red dotted line is the noise-free correct energy for the LiH molecule. The boxplots are the median, first quartile, third quartile, minimum, and maximum of the calculated energy across ten trials, the variation is partially due to noise modeled as Qiskit’s FakeManila backend. The precision of the calculated energy increases with greater pruning. The accuracy also tends to improve.

the most scalable circuit cutting workloads are usually VQA ansatzes [60]. The reason is that ansatzes are usually wide and relatively shallow, meaning they comprise many qubits while having few layers of gates. Furthermore, qubits are loosely connected with two-qubit interactions that match the loosely connected topology of the prototype QCs [35]. For example, in two-local hardware efficient ansatz (HWEA) circuits shown in Figure 1, the number of cuts needed to partition circuits into a constrained number of physical qubits grows linearly versus both width and depth. These HWEA circuits can be used in both quantum chemistry and ML classifier workloads [61], and will be a representative case study in this paper.

Beyond topology, this paper observes that two properties termed determinism and sparsity make VQA ansatz work well with circuit cutting. In recent work, researchers found that parameter pruning is an effective strategy for VQAs, as shown in Figure 2. In a pruning strategy, the rotation angles are tuned to minimize the objective function as is typical for VQA, but as the optimization progresses, the smallest angles are set to zero, in effect removing those rotation gates [42, 61]. Pruning is an effective strategy for training classical neural networks [12, 23, 43] and is also helpful for VQAs in part because it reduces the dimensionality of the optimization problem and noise.

In this work, we argue that pruning confers determinism, which aids in reducing the number of quantum executions needed for a given level of accuracy, and also sparsity, which reduces the classical postprocessing costs.

2.2 Background on Pauli Operators

Here we review the mathematics specific to the quantum circuit cutting strategy. In addition to the state vectors and unitary operators that are important in QC [36, 46, 49, 56], the circuit cutting strategy is formulated in terms of *expectation values* for *observables* specified as *Pauli strings*. These types of values are important in circuit cutting as the expectation values are determined one by one instead of all at once, making circuit cutting more tractable than direct quantum circuit simulation. Furthermore, these types of values are what is gathered from the quantum computer in VQAs.

First, we review quantum *pure* states. The fundamental unit of computation in a quantum computer is a qubit. A single qubit state is represented by the vector $|\psi\rangle = \alpha|0\rangle + \beta|1\rangle$. The *mixed state* is a probabilistic ensemble of pure quantum states. We use a density matrix to represent the mixed state: $\rho = \sum_i p_i |\psi_i\rangle \langle\psi_i|$, where $\langle\psi_i|$ is the conjugate transpose of $|\psi_i\rangle$ and p_i is the probability that the mixed state is in the pure state $|\psi_i\rangle$ and $\sum_i p_i = 1$. The *unitary operation* that applies a unitary gate U to the density matrix description of a quantum state ρ is $\rho^* = U\rho U^\dagger$.

The *expectation value* of the state ρ measured on a certain observable \widehat{O} is $\text{tr}(\rho\widehat{O})$, where tr denotes trace. The trace is an important operation as it underpins our method of decomposing density matrices. Here is a clearer explanation of the expectation value (n is #qubits and $N = 2^n$):

$$\text{tr}(\rho\widehat{O}) = \sum_{i=1}^N (\rho\widehat{O})_{ii} = \sum_{i=1}^N \sum_{j=1}^N (\rho_{ij}\widehat{O}_{ji}) = \sum_{i=1}^N \sum_{j=1}^N (\rho_{ij}\widehat{O}_{ij}^\dagger)$$

\widehat{O}_{ij}^\dagger means the conjugate transpose of \widehat{O}_{ij} .

Now we regard the density matrix ρ as a vector of dimension N^2 . We can decompose it by N^2 *orthogonal bases*. The $4^n = N^2$ *Pauli strings* are such orthogonal basis vectors. The Pauli matrices are

$$I = \begin{bmatrix} 1 & 0 \\ 0 & 1 \end{bmatrix}, \quad X = \begin{bmatrix} 0 & 1 \\ 1 & 0 \end{bmatrix}, \quad Y = \begin{bmatrix} 0 & -i \\ i & 0 \end{bmatrix}, \quad Z = \begin{bmatrix} 1 & 0 \\ 0 & -1 \end{bmatrix}.$$

Pauli strings like $XYXZ$ are the Kronecker (tensor) product of these Pauli matrices in the order $X \otimes Y \otimes X \otimes Z$. The inner product of two different Pauli strings is 0, so the Pauli strings form a complete set of orthogonal bases.

Given a density matrix ρ , the way to decompose it is to find the inner product with the orthonormal basis. Thus, we can write ρ in a new way: $\rho = \sum_{\text{ps} \in \text{Pauli strings}} f(\text{ps}) * \text{ps}$, where ps is one of the Pauli strings like $XY \cdots Z$, and $f(\text{ps})$ is the coefficient corresponding to that Pauli string. $f(\text{ps}) = \text{tr}(\rho\text{ps})/2^n$. One thing to note, since every density matrix is Hermitian (a complex square matrix that is equal to its own conjugate transpose), and each Pauli string is also Hermitian, so when calculating $f(\text{ps}) = \frac{1}{2^n} \sum_{i=1}^N \sum_{j=1}^N (\rho_{ij}\text{ps}_{ij}^\dagger)$, $\rho_{ij}\text{ps}_{ij}^\dagger$ is the conjugate of $\rho_{ji}\text{ps}_{ji}^\dagger$ when $i \neq j$. So, the imaginary part of the coefficient $f(\text{ps})$ is always zero, which means that all coefficients f are real values.

Finally, an example. Consider QFT $|11\rangle$. Its state vector is:

$$\text{QFT}|11\rangle = \frac{1}{\sqrt{2}}(|0\rangle - |1\rangle) \frac{1}{\sqrt{2}}(|0\rangle - i|1\rangle) = |- \rangle |-i \rangle$$

Its density matrix is therefore:

$$|- \rangle \langle - | \otimes |-i \rangle \langle -i | = \frac{1}{4}II - \frac{1}{4}IY - \frac{1}{4}XI + \frac{1}{4}XY$$

The observable Pauli strings are II, IY, XI, XY and their corresponding expectation value coefficients f are $\frac{1}{4}, -\frac{1}{4}, -\frac{1}{4}, \frac{1}{4}$, respectively. We will be using this example in Section 3.

3 Quantum Circuit Cutting: Topology, Determinism, and Sparsity

This section gives a tutorial on the circuit cutting problem. As a contribution from this article, the circuit cutting problem is presented for the first time in the form of a *factor graph exact inference* [40], a well-established task in classical artificial intelligence [18, 39, 51, 57]. This is in contrast to previous work on circuit cutting, which has considered the problem directly using quantum circuits [9, 14, 34, 50, 58, 60] and tensor networks [53, 59] as the underlying abstraction. The advantage of factor graph abstraction is that existing classical AI techniques enable automatic reasoning about determinism and sparsity [17, 19], two properties that this work exploits to make circuit cutting more efficient.

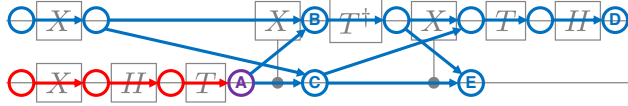
3.1 Execution and Reconstruction Costs due to Topology

The quantum circuit topology and how the circuit is cut into subcircuits have a significant impact on the benefit of circuit cutting and its costs.

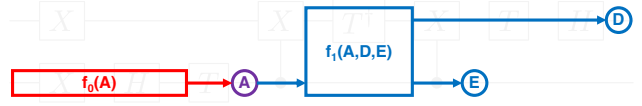
In this work, circuit partitioning and reconstruction are represented as operations on probabilistic graphical models (PGMs). Previous work has used PGMs such as tensor networks [5, 24, 28, 44], Markov networks [7], and Bayesian networks [30] to represent circuits. An example is given in Figure 3, where the graph nodes represent the qubit states and the graph edges represent the quantum gates that modify the qubit states. The circuit cutting task is to partition the graph at nodes into different factors so that the subcircuits can be executed separately on QCs, and the results of the subcircuits are recombined on a classical computer.

A good circuit cutting plan confers benefits. The number of qubits involved in each subcircuit can be kept within the number of qubits available in the quantum computer. The number of gates involved can also be kept within the coherence time frame of the devices. The lower width and depth requirements facilitate the mapping and routing compilation of the circuit to the highest-quality devices.

The penalty of the circuit cutting scheme is the number of subcircuit executions and the cost of reconstruction scales naively as $O(4^k)$, where k is the number of cuts to be made, or more specifically the number of nodes representing the qubit states that partition the circuit [6, 44].



(a) The QFT operation is applied to an $|11\rangle$ initial state set by the X gates. Two-qubit QFT is non-Clifford, as it requires a controlled- S gate. The circuit has been decomposed into a Clifford+ T gate basis where the only two-qubit gates are $CNOT$ gates.



(b) Reconstruction is mathematically equivalent to factor graph exact inference where the red subcircuit forms one factor, the blue subcircuit is another factor, node A is a variable to be eliminated, and nodes D and E are the final query variables.

Figure 3. Directed graphical model representation of cutting, evaluating, and postprocessing a 2-qubit QFT circuit.

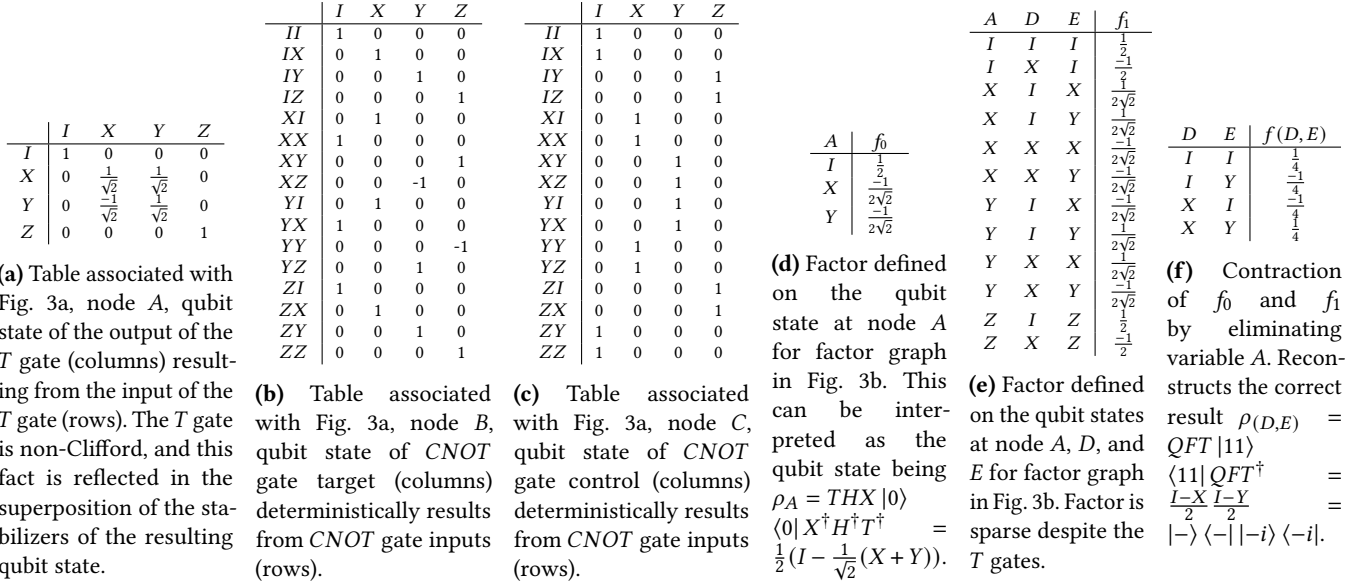


Figure 4. Tables and factors associated with the directed graphical model in Fig. 3a and reconstruction factor graph in Fig. 3b.

All prior work on circuit cutting has focused on these costs and benefits related to the quantum circuit topology.

3.2 Execution Costs due to Determinism

Although previous work in circuit cutting focused on the topology of quantum circuits, the stabilizer and Clifford structure of the circuits are an equally important aspect of the subcircuits execution cost. The ability to predict, compile, and query this structure is key to this work and leads to efficiencies in the running of QC experiments and to enhancing the accuracy of the results. The effect is especially relevant to NISQ VQA ansatzes with parameter pruning.

Quantum circuits that contain only stabilized states and Clifford operators are known to be classically easy to simulate in polynomial time and memory requirements [1, 10, 11, 25]. In the PGM representation proposed in this paper, the distinction between Clifford and non-Clifford is equivalent to the concept of *determinism*. The classic example of determinism in graphical models imagines a scenario in which if a sprinkler is on, the grass is certain to be wet [57]. This

knowledge can be captured as a direct entailment without involving any probabilities. It is a certainty embedded in an otherwise probabilistic model.

In the PGM representation of circuits, Clifford gates are analogous to direct entailment, whereas only non-Clifford gates introduce expectation value coefficients. For example, the Hadamard gate (which is Clifford) deterministically interchanges states stabilized by the Pauli X and Z operators. The Clifford two-qubit $CNOT$ gate shown in Figs. 4b and 4c shows that exactly one stabilizer outcome has a non-zero coefficient for each of the stabilizer inputs. Therefore, the Clifford Hadamard and $CNOT$ gates represent deterministic transitions between the Pauli bases. The prototypical non-Clifford T gate shown in Figure 4a maps the input Pauli X and Y bases to superpositions of the output Pauli X and Y bases; these mappings introduce non-trivial coefficients.

Classical AI provides a set of *knowledge compilation* techniques that efficiently count, enumerate, and calculate probabilities of events in PGMs [18, 19, 38]. We apply these techniques to encode determinism, compile causal information,

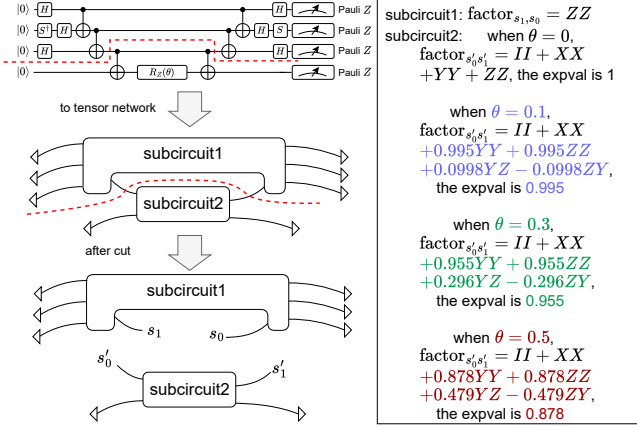


Figure 5. Varying non-Clifford rotation gate angles only affects numerical coefficients while the Pauli bases remain deterministically unchanged. The circuit shows a Pauli XYZ evolution gate on initial state $|0000\rangle$ and measurement of the expectation value on observable $ZZZZ$.

and query this information as needed to drive the circuit cutting strategy.

Knowledge of the Clifford structure can be exploited for more efficient experiment execution. For example, the subcircuit for $f_1(A, D, E)$ in Figure 3b needs to be executed with various initializations for the qubit state A and measurements on the qubit states D and E in Figure 4e; knowing the valid output states of A from the subcircuit $f_0(A)$ would reveal that experiments that initialize A as Pauli Z are unnecessary. The reduction in the number of experiments that actually have to be run ripples through the chain of subcircuits.

Knowledge of the Clifford structure can also be exploited to increase the accuracy of reconstructed results. For example, the possible Pauli strings of the reconstructed result are in Figure 4f where only four out of 16 bases are non-zero; any strings that do not belong to this set are due to noise, and omitting those strings forms a new kind of error mitigation.

In fact, as shown in Figure 5, in VQAs that we claim are especially suited for circuit cutting, only the non-Clifford gates in the ansatz circuit expand the set of Pauli strings for the input and output of the subcircuit. The variation of the rotation angles θ on the non-Clifford gates as the variational algorithm executes only amounts to changes in the observable weights of the Pauli strings. As the angles are increasingly pruned according to Figure 2, the set of nonzero Pauli strings decreases, decreasing the number of experiments needed and strengthening the error mitigation effect. These ideas are evaluated in Sections 4.2 and 4.3.

3.3 Reconstruction Costs due to Sparsity

The fact that the Clifford structure of quantum circuits creates structure in subcircuit inputs and outputs makes the data for the reconstruction postprocessing very sparse. The

sparsity of the data collected from the subcircuit evaluation is clearly seen in Figure 4e. Of the $4^3 = 64$ possible Pauli strings for the input and output combinations of the f_1 subcircuit, only 12 are consistent with the Clifford structure of the subcircuit and have a non-zero expectation value.

One reason that previous work may have overlooked this sparsity in the data and failed to exploit it may be because the sparsity is only obvious when expressed in the stabilizer Pauli string basis. Previous work in circuit cutting represented the results of subcircuit executions on the basis of subcircuit input qubit initialization states [53], where the sparsity is not obvious.

Whereas all previous work on quantum circuit cutting has treated this task using conventional matrix and tensor multiplication, a contribution of this work is to process these data as sparse tensor contraction using hashes. The improved algorithm leads to a reduced number of floating-point operations and a reduced memory footprint needed for post-processing. These ideas are evaluated in Sections 5.2 and 5.3.

4 Efficient Circuit Cutting Execution and Noise Mitigation Exploiting Determinism

Prior work in quantum circuit cutting raised concerns that the number of subcircuit executions is non-scalable. In this section, we first review how the subcircuit execution cost arises due to the input and output combinations needed to perform quantum state tomography. That naive baseline approach is what is implemented in standard circuit cutting frameworks such as `qiskit-addon-cutting` [8]. In NISQ VQA ansatzes with pruned parameters, one can perform significantly better than the baseline. Once the ansatz topology and cutting plan are set, non-zero observations can be deterministically predicted via extended stabilizer simulation. Exploiting the determinism leads to either fewer subcircuit executions, tomography results with greater precision, or both. Finally, we show that our approach matches the error mitigation and efficiency demonstrated in an orthogonal approach termed *shadow tomography* [16, 29].

4.1 Background: Execution Inputs and Outputs

For a subcircuit with n input edges and m output edges, it is necessary to try the four initialization states $\{|0\rangle\langle 0|, |1\rangle\langle 1|, |+\rangle\langle +|, |i\rangle\langle i|\}$ for each input edge, and for each output edge, it is necessary to try the three observables $\{X, Y, Z\}$ for complete tomography of the quantum state. Take Figure 5 for example, where that VQA ansatz circuit partitioning plan has both mid-circuit measurements and mid-circuit initializations. Subcircuit 1 has an input edge s_0 and an output edge s_1 . Subcircuit 2 has an input edge s'_0 and an output edge s'_1 .

Therefore, we need to map the subcircuit input Pauli strings $\{I, X, Y, Z\}$ to the actual $\{|0\rangle\langle 0|, |1\rangle\langle 1|, |+\rangle\langle +|, |i\rangle\langle i|\}$ states to which qubits can be initialized. There are $4^n 3^m$ circuit input output settings and, without further knowledge of the ansatz topology, one would have to naively evaluate

all the settings on the quantum computer. Let the function g record the results.

$$\begin{aligned} g(s_0, s_1, \dots, s_{n-1}, s_n, \dots, s_{n+m-1}) &\in [-1, 1], \\ s_i &\in \{|0\rangle\langle 0|, |1\rangle\langle 1|, |+\rangle\langle +|, |i\rangle\langle i|\}, 0 \leq i < n \\ s_j &\in \{I, X, Y, Z\}, n \leq j < n + m. \end{aligned}$$

Notice that g is a linear function, and we have:

$$\begin{aligned} I &= |0\rangle\langle 0| + |1\rangle\langle 1| \\ X &= 2|+\rangle\langle +| - |0\rangle\langle 0| - |1\rangle\langle 1| \\ Y &= 2|i\rangle\langle i| - |0\rangle\langle 0| - |1\rangle\langle 1| \\ Z &= |0\rangle\langle 0| - |1\rangle\langle 1| \end{aligned}$$

As a result, we can let f be a new function that transforms s_0 to the $\{I, X, Y, Z\}$ basis. Let $f(s_0, \dots)$ mean $f(s_0, s_1, \dots, s_{n+m-1})$:

$$\begin{aligned} f(I, \dots) &= g(|0\rangle\langle 0|, \dots) + g(|1\rangle\langle 1|, \dots) \\ f(X, \dots) &= 2g(|+\rangle\langle +|, \dots) - g(|0\rangle\langle 0|, \dots) - g(|1\rangle\langle 1|, \dots) \\ f(Y, \dots) &= 2g(|i\rangle\langle i|, \dots) - g(|0\rangle\langle 0|, \dots) - g(|1\rangle\langle 1|, \dots) \\ f(Z, \dots) &= g(|0\rangle\langle 0|, \dots) - g(|1\rangle\langle 1|, \dots) \end{aligned}$$

Now we have successfully transformed the first dimension. Repeating this for the other $n - 1$ dimensions, we will get a function f with every $s_i \in \{I, X, Y, Z\}$. f is the factor for the entire subcircuit that we discussed in Section 2.2 and Figures 4d, 4e, and 4f. We record the function f as a tensor of dimensions $n + m$. The extent of each dimension is four. In each iteration, the time complexity of transforming the basis is linear to the size of the tensor, $O(4^{n+m-1})$. There are n iterations, so the time complexity of performing the entire basis transformation is $O(n4^{n+m-1})$. This represents the baseline cost of subcircuit execution in circuit cutting [53].

4.2 Efficient Execution with Known Subcircuit Pauli Strings

Here, we exploit knowledge of the correct input and output pairs from the Clifford structure of pruned VQA subcircuits. Compared to the baseline approach implemented in standard circuit cutting frameworks such as *qiskit-addon-cutting* [8], exploiting this knowledge leads to tomography results with greater precision using fewer subcircuit executions.

Representative VQA workload: We study the hardware efficient ansatz consisting of layers of R_Y , R_Z , and CZ gates shown in Figure 1 as a standard VQA ansatz that is relevant for both chemistry and quantum machine learning [35]. HWEA(N,d,n) means cutting an N-qubit d-layer HWEA into n-qubit subcircuits. We keep the qubit count constant at eight qubits and later scale our approach to 200+ qubits in Section 5. The circuits are cut into subcircuits of width five, such that two cutting points are needed for each ansatz layer.

Baseline versus our approach: The *qiskit-addon-cutting* package (we use the latest version 0.9.0 in this paper), previously known as the Circuit Cutting Toolbox, represents

the baseline approach that does not know the Clifford structure of the subcircuits. The baseline approach creates 8 basis elements at each cutting point: $I_0, I_1, X_0, X_1, Y_0, Y_1, Z_0, Z_1$. Therefore, for k cutting points, the total number of experiments is distributed across 8^k combinations of input initializations and output measurements. Once all experiments are executed, the baseline approach reconstructs the quasi-probability decomposition for the subcircuit.

Our work uses the approach described in Section 3.2 to distribute the total number of experiments over only the subcircuit initializations and measurements that will help the reconstructed state converge to the accurate solution.

As shown in Figure 6, our approach achieves greater precision than the naive approach for a given number of total experiments. In other words, our approach converges to the same level of precision in fewer total experiments.

Trends across ansatz gate pruning: As the pruning ratio grows, the proportion of non-Clifford gates would be smaller, resulting in fewer non-zero Pauli strings in subcircuits. Our work more efficiently distributes the total number of experiments to fewer correct circuit initialization and measurement combinations, leading to more precise reconstructed values. The baseline approach cannot take advantage of the fewer combinations that result from gate pruning.

Trends across ansatz layer depth: The number of cutting points in the circuit grows linearly with the depth of the ansatz, and the total execution cost of the circuit cutting scheme is understood to be exponential relative to the number of cutting points. This penalty is obvious for the baseline approach, where for a given budget of the total number of experiments, the limited number of samples for each observable leads to large variances in the reconstructed expectation value. For four-layer ansatzes shown in Figures 6g, 6h, and 6i, many trials for the baseline approach conclude with an expectation value lower than the correct value due to the large variance, in violation of Ritz’s variational principle. In our approach, deterministic knowledge of the input and output pairs samples only the correct combinations.

4.3 Error Mitigation with Known Subcircuit Pauli Strings

As seen in Figure 6, the medians of our reconstructed expectation values are closer to the true value when compared against *qiskit-addon-cutting*. This means that our approach has greater accuracy, in addition to greater precision, than the baseline approach. In this section, we show that our accuracy improvement matches an orthogonal quantum state tomography method termed classical shadow tomography [16, 29]. We discuss the source of the error mitigation.

VQA workload: We focus this error mitigation study on an eight-qubit two-layer HWEA circuit. The restriction of

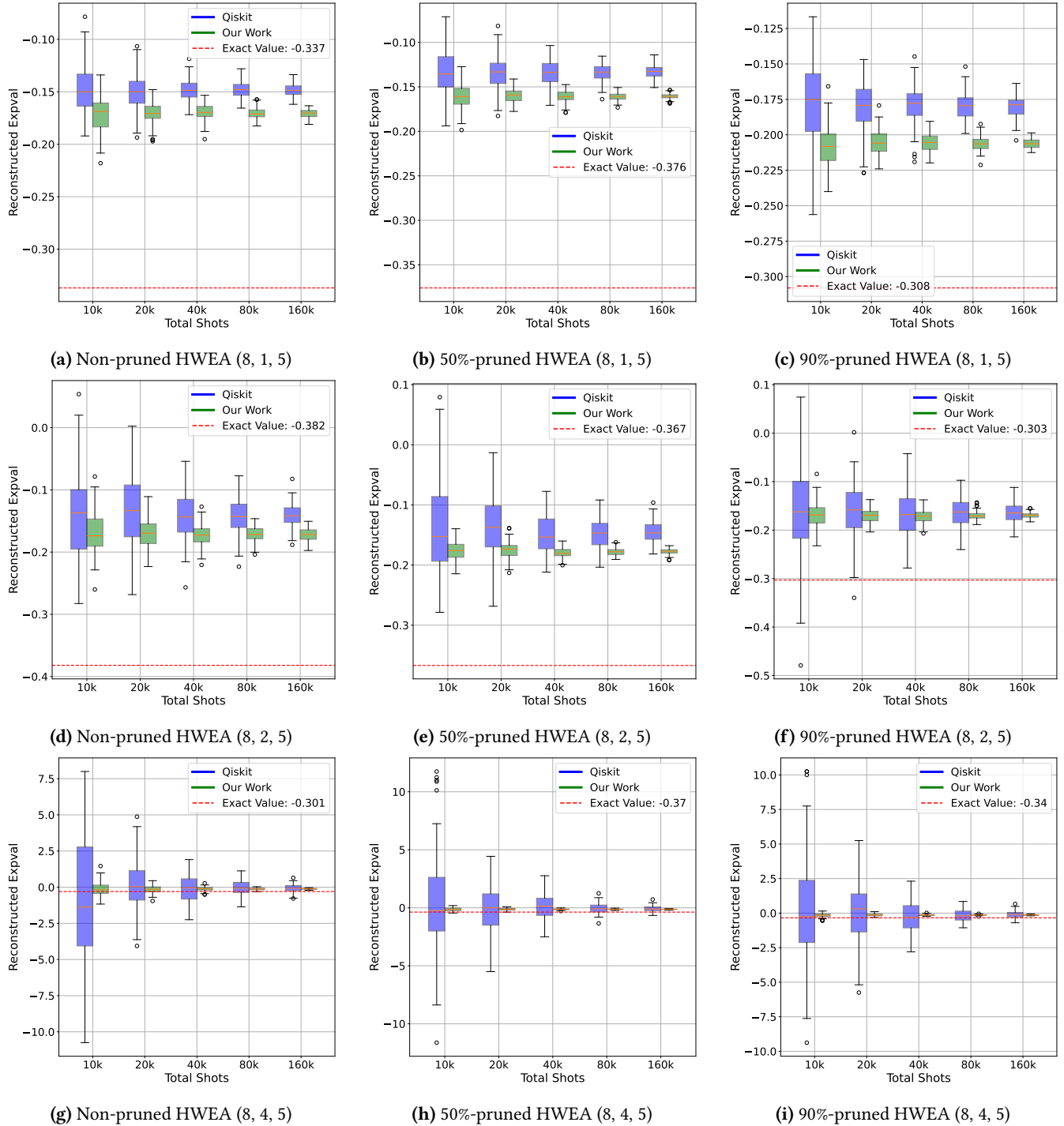
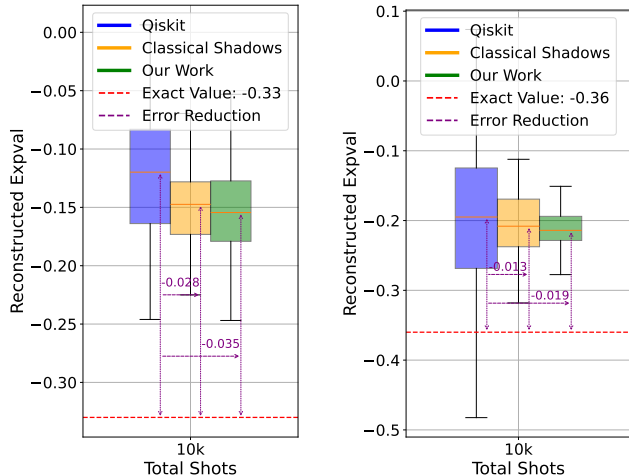


Figure 6. Efficient subcircuit execution with deterministically known circuit initializations and measurements. *In the plots*, the vertical axes are the reconstructed ansatz expectation value. The horizontal axes are the total number of shots distributed across input initializations and output measurement combinations. The red dotted line is the correct noise-free expectation value for each eight-qubit ansatz circuit. The data series are our approach versus the baseline approach for reconstructing the expectation value from the five-qubit subcircuits. The boxplots summarize the reconstructed expectation value from 100 trials. The variation around the median and the gap from the median to the correct value are due to the noise model from the FakeManila backend in IBM Qiskit. *Horizontally across the plots*, the smallest non-Clifford rotation gate angles are progressively pruned as the VQA progresses. *Vertically down the plots*, the scheme is tested on two- and four-layer ansatzes.



(a) Non-pruned HWEA (8,2,5). Each subcircuit involves one upstream cut and one downstream cut. Since the tensor lacks sparsity, we must conduct all 12 experiments per subcircuit, using 4 bases for the downstream cut and 3 bases for the upstream cut. Our approach matches the error mitigation of classical shadows in terms of shot efficiency when there is no pruning. (b) 90%-pruned HWEA (8,2,5). Our approach uses determinism to avoid examining every basis. This reduces the combinations we try to just 12, as opposed to 24, thereby doubling the number of shots per combination compared to the non-pruned scenario. The denser sampling in our method converges to greater precision in comparison to classical shadows.

Figure 7. Comparison of the error mitigation capabilities of our approach, classical shadows, and *qiskit-addon-cutting*. We limited our tests to a total of 10k shots, and the boxplot definitions are consistent with those in Figure 2. Purple arrows indicate the gap between the median values and the noise-free correct value, representing the absolute error. Both our method and classical shadows achieve an equivalent level of error reduction, yielding more accurate results than *qiskit-addon-cutting*.

the experiment to this circuit is due to the difficulty in simulating the classical shadow tomography procedure. Although both our approach and *qiskit-addon-cutting* can batch the simulation shots into the subcircuit input and output combinations, the classical shadow tomography approach selects a new input initialization and output measurement basis after every single measurement.

Baseline versus our approach: Classical shadow tomography approximates the quantum state density matrix using a few shots by randomly selecting a Pauli basis for each shot, unlike standard tomography that measures on every Pauli basis. This process is similar to applying an invertible depolarizing channel. The average density matrix estimated from this method aligns with the true density matrix, allowing for accurate estimation with minimal shots. However, with

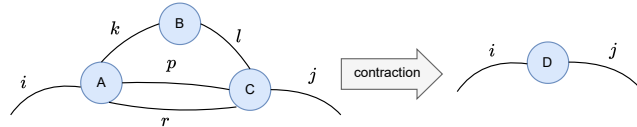


Figure 8. Example of tensor contraction.

a large number of shots, it offers no advantage over standard tomography. While the classical shadows approach is state-of-the-art, it still measures observables with zero expectation value, and those shots contribute nothing to state reconstruction. Our approach elides those empty shots.

Trends across ansatz gate pruning: In Figure 7, our work and the classical shadow approach are at the same level of mitigating errors compared *qiskit-addon-cutting*. When there is no pruning, our work matches the classical shadow tomography in terms of precision. When there is 90% pruning, our work beats the classical shadow approach in terms of precision.

5 Efficient Circuit Cutting Reconstruction Postprocessing Exploiting Sparsity

Prior work in quantum circuit cutting also raised concerns that the cost of reconstructing expectation values across the subcircuits using a classical computer is non-scalable. In this section, we review how the classical post-processing cost arises due to the need to perform a tensor network contraction. The difficulty of the contraction task is strongly impacted by the choice of the contraction order. Prior work focused on using state-of-the-art heuristics for finding a contraction order via libraries such as Cotengra. The contraction task is then performed using GPUs using libraries such as cuQuantum and cuTENSOR. In our work, we once again show that in NISQ VQA ansatzes with pruned parameters, one can exploit sparsity in the tensors to beat the baseline. Exploiting sparsity leads to reductions in the operations needed for reconstruction, reduces the memory footprint, and expands the size of NISQ VQA circuits suitable for circuit cutting to sizes previously thought to be intractable.

5.1 Background: Reconstruction Tensor Contraction

Here, we discuss why the tensor contraction task arises. In the discussion about quantum circuit cutting so far, the quantum computer has returned the expectation values for the Pauli string observables for each subcircuit. These expectation values correspond to the weights of the factors in the graphical model presented in Figures 3b, 4d, and 4e. The classical host computer now has to eliminate the variables representing the qubit states where the original quantum circuit was partitioned, to reconstruct the expectation values for only the output qubit states represented in Figure 4f. In prior work on circuit cutting, expectation values are stored

as tensors and the topology of how subcircuits are connected is represented as a tensor network. Eliminating internal variables from the tensor network is termed tensor network contraction.

Tensor contraction is high-dimensional matrix multiplication. Take Figure 8 as an example. We have three tensors A , B , and C . After contraction, we get a tensor D that has only two edges i and j .

$$D_{ij} = \sum_{k,l,p,r} A_{ikpr} B_{kl} C_{prlj}$$

Tensor sizes grow exponentially with the number of open edges. In circuit cutting, the extent of each edge is four representing the four Pauli bases, such that the size of the tensor with k edges is 4^k . This represents a naive cost of the tensor contraction task.

Tensor network contraction can be done via the *einsum* operation in NumPy, though the state-of-the-art is to use GPU libraries such as cuTENSOR, or more specifically the cuQuantum library part of Nvidia CUDA-Q [21].

Notice in the example above that the order in which A , B , and C are eliminated has no effect on the correctness of the outcome D , but it does have a significant effect on the computational cost. For the much trivial case of matrix chain multiplication, where all tensors are rank-two matrices such that the tensor network is just a linear chain, the optimal chain matrix multiplication task has a log-linear-time algorithm for finding the multiplication order. The optimal contraction ordering for general tensor networks is in contrast NP-Hard. Here, we use the state-of-the-art Cotengra library to provide heuristic orderings [26].

5.2 Reduced Operations via Sparse Contraction

As previewed in Section 3.3, the factors and tensors in the circuit cutting task are sparse, and this is especially true for NISQ VQA circuits with parameter pruning. Here we show that the sparsity has significant impact on the number of floating point operations needed for circuit cutting postprocessing, and this effect is orthogonal to the choice of tensor network contraction order.

NISQ versus beyond-NISQ circuit cutting workloads:

We study the effect of sparsity on the feasibility of cutting two main types of quantum circuits.

For beyond-NISQ workloads, we select the quantum Fourier transform (QFT)[31] as a representative circuit. These circuits are characteristically deep and have dense qubit interactions, leading to all-to-all connectivity. Figure 9a shows that even for these circuits, the subcircuit tensors become increasingly sparse. Because QFT is by definition difficult to partition with few cuts, the QFT problem sizes that circuit cutting can handle are necessarily narrow with few qubits. In the memory footprint limitations in our study, we are limited to reconstructing a seven-qubit QFT that requires 14 cuts.

Algorithm 1 Sparse Tensor Contraction

```

1: procedure SPARSE_CONTRACT(sp_tensor1, sp_tensor2)
2:   if sp_tensor1.size() > sp_tensor2.size() then
3:     swap(sp_tensor1, sp_tensor2)
4:   end if
5:   HashTable<index, entry> hash_map
6:   HashTable<index, value> result
7:   List<entry> sp_tensor_result
8:   # Preprocessing the index transformation
9:   for entry in sp_tensor1 do
10:    entry.common_index ← transform1(entry.index)
11:    entry.uncommon_index ← transform2(entry.index)
12:   end for
13:   for entry in sp_tensor2 do
14:    entry.common_index ← transform3(entry.index)
15:    entry.uncommon_index ← transform4(entry.index)
16:   end for
17:   # Build the hash table
18:   for entry1 in sp_tensor1 do
19:     hash_map[entry1.common_index].append(entry1)
20:   end for
21:   # Contract
22:   for entry2 in sp_tensor2 do
23:     matched_entries ← hash_map[entry2.common_index]
24:     for entry1 in matched_entries do
25:       new_index ← entry1.uncommon_index
26:       +entry2.uncommon_index
27:       result[new_index] += entry1.value * entry2.value
28:     end for
29:   end for
30:   sp_tensor_result ← to_list(result)
31:   return sp_tensor_result
32: end procedure

```

For NISQ workloads, we again use the HWEA as a representative circuit that has uses in Hamiltonian simulation and machine learning. As shown in Figure 9b and 9c, the sparsity of subcircuit tensors are controlled by the parameter pruning as expected, but also by the ansatz layer count, with deeper circuits having sparser tensors. The HWEA circuit cutting workload can scale out to 200-qubits and six layers before reaching the memory limitations set in this study.

Additional workloads are studied in Table 1 to confirm the generality of our observation about sparsity.

Baseline versus our approach: Our approach for circuit cutting postprocessing uses sparse tensor contraction, as described in Algorithm 1. Instead of storing tensors in a flat format, sparse tensors use a list of index-value pairs, storing only non-zero values. When contracting two sparse tensors, we build a hash table for the first tensor and process the second tensor by matching entries. Our sparse algorithm is run on an AMD EPYC 7313 16-Core Processor.

For the baseline, we use Cotengra to plan a near-optimal contraction order [26], and contraction is done using cuQuantum [21] running on a GeForce GTX 2080ti. This represents the state-of-the-art backend for reconstruction.

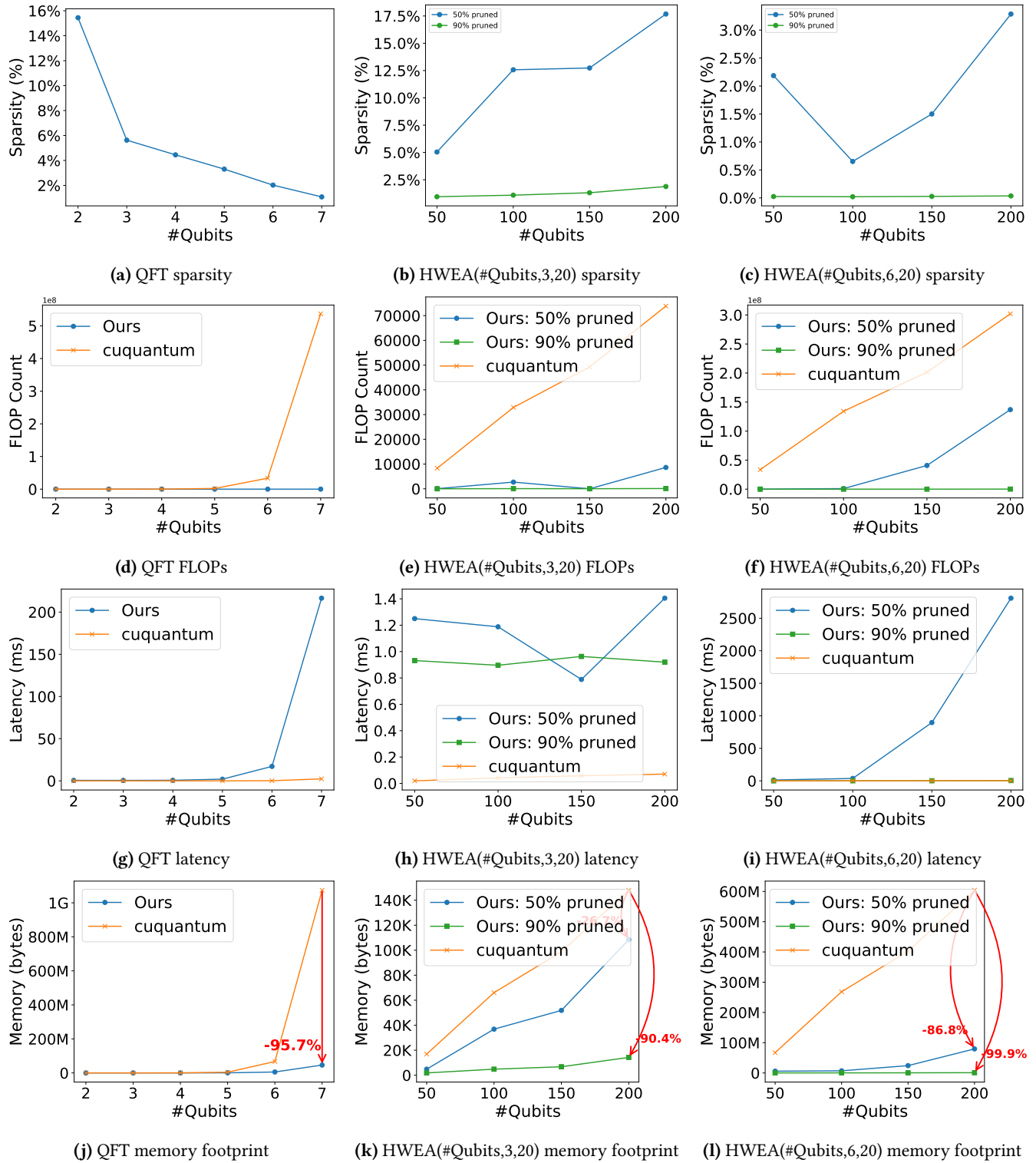


Figure 9. The plot shows the postprocessing costs comparison between GPU cuQuantum implementation and our proposed sparse contraction approach. The x-axis is the number of qubits. The y-axis is the sparsity and performance metrics: FLOP count, latency, and memory footprint. The orange curves are cuQuantum. The blue and green curves in HWEA are our method when the pruning ratio is 50% and 90%. In QFT, there's no pruning so we use blue curves to represent our method. As the number of qubits grows, our method outperforms cuQuantum in FLOP count and memory footprint but is outperformed by cuQuantum in latency. In HWEA, the more pruning ratio our method has better performance. Our method's memory footprint reduction depends on sparsity. When sparsity is around 2%, the reduction can be around 90%.

Trends across ansatz gate pruning: As shown in Figures 9d, 9e, and 9f, our approach is able to perform the expectation value reconstruction in fewer floating point operations (FLOPs) avoiding zero operations due to sparsity. The FLOP count of our proposed method would be around $(\text{sparsity})^2$ of that of cuQuantum. The effect is more significant as the VQA ansatz parameters are pruned.

Trends across qubit count: Taking advantage of sparsity allows us to scale the HWEA workload to at least 200 qubits, which is at or beyond the qubit count circuit width attempted in previous work. While prior work measured qubit count as a primary measure of whether circuit cutting can scale, the more nuanced viewpoint is that whether a circuit is easy to cut depends entirely on the type of circuit, as evidenced in the vastly different scalability of QFT vs. HWEA.

Trends across ansatz layer depth: The more significant controlling factor for whether circuit cutting can scale for NISQ VQAs is the layer count in the ansatzes. The HWEA workload scales to six layers to match the order of magnitude number of FLOPs for the QFT workload. Figures 9g, 9h, and 9i show that while our sparse approach incurs fewer FLOPs, the reduction in operations does not translate to improvements in wall-clock latency due to the parallelism offered in the GPU, while our hash-based approach requires pointer chasing. However, these workloads are completed within seconds, and the primary limitation of workload scalability is actually the required memory footprint.

5.3 Reduced Memory Footprint via Sparse Contraction

Figures 9j, 9k, and 9l show the memory footprint reduction due to our sparse approach. We can see that 2% sparsity can reduce the memory footprint by around $\sim 90\%$ compared to cuQuantum.

The memory footprints are measured from the program implementations and checked against analytical models. For our sparse implementation, we calculate the memory footprint of the two hash tables and three sparse tensor lists in Algorithm 1. We implement the function in C++ and we use vector and unordered_map from the C++ standard template library as a list and hash table. The memory footprints are modeled analytically as follows. Let A be the tensor size of a subcircuit1, B be that of a subcircuit2, and D that of the contracted tensor. Without taking advantage of the sparsity, the memory footprint of cuQuantum is $4(A + B + D)$ bytes, where 4 is the byte size of the floating point type. Let the sparsity of the three tensors be a, b, d , respectively. The memory footprint of our approach taking advantage of the sparsity is

$$16(aA + bB + dD) + \text{hash_table_overhead} \times [\min(aA, bB) + dD]$$

The first term describes the memory footprint of the three lists of entries, and the second term describes the memory footprint of the two hash tables. The 16 in the first term

is the size of the entry type. In practice, the second term is negligible compared to the first term because the contraction path finder will always let us contract a small-sized tensor with a large-sized tensor.

Using the analytical model, we show additional experiments on memory footprint reduction for a benchmark of workloads shown in Table 1.

6 Related Work in Distributed QC

Distributed quantum computing is a set of techniques to combine the capabilities of multiple QCs [2]. Techniques include physically networking multiple QCs together so that qubits move between systems [37, 41, 47, 62], or entanglement between systems can be established before program runs begin [4]. A third strategy called circuit cutting is the use of classical computing to combine the results of multiple QCs, and is the focus of this paper.

Circuit cutting confers advantages and has several practical challenges. The mathematics for cutting quantum circuits was proposed by Peng *et al.* [53] and implemented for the first time by Tang *et al.* [59, 60]. Numerous subsequent studies address different challenges in the circuit cutting strategy. These include the decision on where to cut quantum circuits to fit the subcircuits into hardware constraints [34]. The cut identification problem has been extended to consider both time-wise wire cuts and space-wise gate cuts [9, 50]. When the subcircuits are run, the resulting quantum state needs to be observed by efficient tomography [14, 16]. Finally, studies have been performed to reduce the reconstruction cost by approximation [15] and by identifying purely Clifford subcircuits [58]. Table 2 summarizes the most relevant prior work and the problem sizes they test.

7 Conclusion

This paper explores the influence of topology, determinism, and sparsity on quantum circuit cutting costs, with a focus on determinism and sparsity for subcircuit evaluation and reconstruction. Subcircuits are transformed into factor graphs, using knowledge compilation to identify minimal initialization and measurement sets based on non-zero input-output Pauli string pairs. This guides a more efficient tomography method, reducing zero-valued outputs and aiding error mitigation. Subcircuit factors are treated as tensors, and in reconstruction, tensors are contracted to exploit sparsity, reducing memory use. We compare our subcircuit execution to *qiskit-addon-cutting* and classical shadows, and our reconstruction postprocessing to cuQuantum, showing clear advantages.

References

- [1] Scott Aaronson and Daniel Gottesman. Improved simulation of stabilizer circuits. *Phys. Rev. A*, 70:052328, Nov 2004.
- [2] David Barral, F. Javier Cardama, Guillermo Díaz, Daniel Faílde, Iago F. Llovo, Mariamo Mussa Juane, Jorge Vázquez-Pérez, Juan Villasuso, César Piñeiro, Natalia Costas, Juan C. Pichel, Tomás F. Pena, and

Workload	#qubits	#cuts	Sparsity	cuQuantum memory footprint	Our work's memory footprint	Memory footprint reduction
UCCSD	12	12	10.3%	128 MB	26.5 MB	79.3%
UCCSD	14	14	0.56%	2 GB	22.9 MB	98.88%
QFT	20	20	0.0009%	8 TB	190 MB	99.998%
GHZ	10	10	0.1%	8 MB	17 KB	99.8%
GHZ	20	20	0.00003%	8 TB	5 MB	99.999%
Erδος QAOA	20	20	0.00005%	8 TB	37.7 MB	99.999%
Supremacy [28]	16	16	1.0 %	34 GB	714 MB	97.9%
Sycamore [52]	16	16	0.001 %	34 GB	1 MB	99.997%

Table 1. Memory footprint comparison between cuQuantum and our sparse approach for different circuit workloads.

Prior work	Wire Cut	Gate Cut	NISQ workloads	Beyond-NISQ workloads	Open-sourced
CutQC [60]	Yes	No	HWEA (100 qubits), Supremacy (100 qubits), Approximate QFT (100 qubits)	Grover (59 qubits), BV (100 qubits), Adder (100 qubits)	Yes
FitCut [34]	Yes	No	HWEA (100 qubits), Supremacy (72 qubits)	BV(120 qubits), Adder(80 qubits)	Not yet
Integrated Qubit Reuse and Circuit Cutting [50]	Yes	Yes	QAOA (50 qubits), Supremacy (40 qubits)	QFT (30 qubits), Adder (40 qubits)	Not yet
qiskit-addon-cutting [8]	Yes	Yes	N.A.	N.A.	Yes
This work	Yes	No	HWEA (200 qubits)	QFT (20 qubits) etc.	Will be

Table 2. Selected previous works that implemented and a circuit cutting framework.

- Andrés Gómez. Review of distributed quantum computing. from single qpu to high performance quantum computing, 2024.
- [3] Harun Bayraktar, Ali Charara, David Clark, Saul Cohen, Timothy Costa, Yao-Lung L. Fang, Yang Gao, Jack Guan, John Gunnels, Azzam Haidar, Andreas Hehn, Markus Hohnerbach, Matthew Jones, Tom Lubowe, Dmitry Lyakh, Shinya Morino, Paul Springer, Sam Stanwyck, Igor Terentyev, Satya Varadhan, Jonathan Wong, and Takuma Yamaguchi. cuquantum sdk: A high-performance library for accelerating quantum science, 2023.
- [4] Charles H. Bennett, Gilles Brassard, Claude Crépeau, Richard Jozsa, Asher Peres, and William K. Wootters. Teleporting an unknown quantum state via dual classical and einstein-podolsky-rosen channels. *Phys. Rev. Lett.*, 70:1895–1899, Mar 1993.
- [5] Jacob Biamonte and Ville Bergholm. Tensor networks in a nutshell, 2017.
- [6] Hans L. Bodlaender. Treewidth: Characterizations, applications, and computations. In *Proceedings of the 32nd International Conference on Graph-Theoretic Concepts in Computer Science, WG'06*, page 1–14, Berlin, Heidelberg, 2006. Springer-Verlag.
- [7] Sergio Boixo, Sergei V. Isakov, Vadim N. Smelyanskiy, and Hartmut Neven. Simulation of low-depth quantum circuits as complex undirected graphical models, 2018.
- [8] Agata M. Brańczyk, Almudena Carrera Vazquez, Daniel J. Egger, Bryce Fuller, Julien Gacon, James R. Garrison, Jennifer R. Glick, Caleb Johnson, Saasha Joshi, Edwin Pednault, C. D. Pemmaraju, Pedro Rivero, Ibrahim Shehzad, and Stefan Woerner. Qiskit addon: circuit cutting. <https://github.com/Qiskit/qiskit-addon-cutting>, 2024.
- [9] Sebastian Brandhofer, Ilia Polian, and Kevin Krsulich. Optimal partitioning of quantum circuits using gate cuts and wire cuts. *IEEE Transactions on Quantum Engineering*, 5:1–10, 2024.
- [10] Sergey Bravyi, Dan Browne, Pdraic Calpin, Earl Campbell, David Gosset, and Mark Howard. Simulation of quantum circuits by low-rank stabilizer decompositions. *Quantum*, 3:181, September 2019.
- [11] Sergey Bravyi and David Gosset. Improved classical simulation of quantum circuits dominated by Clifford gates. *Phys. Rev. Lett.*, 116:250501, Jun 2016.
- [12] Han Cai, Chuang Gan, Tianzhe Wang, Zhekai Zhang, and Song Han. Once for all: Train one network and specialize it for efficient deployment. In *International Conference on Learning Representations*, 2020.
- [13] Yudong Cao, Jonathan Romero, Jonathan P. Olson, Matthias Degroote, Peter D. Johnson, Mária Kieferová, Ian D. Kivlichan, Tim Menke, Borja Peropadre, Nicolas P. D. Sawaya, Sukin Sim, Libor Veis, and Alán Aspuru-Guzik. Quantum chemistry in the age of quantum computing. *Chemical Reviews*, 119(19):10856–10915, 10 2019.
- [14] D. T. Chen, E. H. Hansen, X. Li, A. Orenstein, V. Kulkarni, V. Chaudhary, Q. Guan, J. Liu, Y. Zhang, and S. Xu. Online detection of golden circuit cutting points. In *2023 IEEE International Conference on Quantum Computing and Engineering (QCE)*, pages 26–31, Los Alamitos, CA, USA, sep 2023. IEEE Computer Society.
- [15] Daniel Chen, Betis Baheri, Vipin Chaudhary, Qiang Guan, Ning Xie, and Shuai Xu. Approximate quantum circuit reconstruction. In *2022 IEEE International Conference on Quantum Computing and Engineering (QCE)*, pages 509–515, 2022.
- [16] Daniel Tzu Shiu Chen, Zain Hamid Saleem, and Michael Alexandrovich Perlin. Quantum circuit cutting for classical shadows. *ACM Transactions on Quantum Computing*, 5(2), jun 2024.
- [17] Adnan Darwiche. New advances in compiling cnf to decomposable negation normal form. In *Proceedings of the 16th European Conference on Artificial Intelligence, ECAI'04*, page 318–322, NLD, 2004. IOS Press.
- [18] Adnan Darwiche. *Modeling and Reasoning with Bayesian Networks*. Cambridge University Press, 2009.
- [19] Adnan Darwiche and Pierre Marquis. A knowledge compilation map. *J. Artif. Int. Res.*, 17(1):229–264, sep 2002.
- [20] Advait Deshpande. Assessing the quantum-computing landscape. *Commun. ACM*, 65(10):57–65, sep 2022.
- [21] Leo Fang, ahehn nv, hbbayraktar, and sam stanwyck. Nvidia/cuquantum: cuquantum v22.05.0, May 2022.
- [22] Edward Farhi, Jeffrey Goldstone, and Sam Gutmann. A quantum approximate optimization algorithm, 2014.
- [23] Jonathan Frankle and Michael Carbin. The lottery ticket hypothesis: Finding sparse, trainable neural networks. In *International Conference on Learning Representations*, 2019.

- [24] E. Schuyler Fried, Nicolas P. D. Sawaya, Yudong Cao, Ian D. Kivlichan, Jhonathan Romero, Alán Aspuru-Guzik, and Itay Hen. qtorch: The quantum tensor contraction handler. *PLoS ONE*, 13(12), 12 2018.
- [25] D Gottesman. The Heisenberg representation of quantum computers. 6 1998.
- [26] Johnnie Gray and Stefanos Kourtis. Hyper-optimized tensor network contraction. *Quantum*, 5:410, March 2021.
- [27] Torsten Hoefler, Thomas Häner, and Matthias Troyer. Disentangling hype from practicality: On realistically achieving quantum advantage. *Commun. ACM*, 66(5):82–87, apr 2023.
- [28] Cupjin Huang, Fang Zhang, Michael Newman, Junjie Cai, Xun Gao, Zhengxiong Tian, Junyin Wu, Haihong Xu, Huanjun Yu, Bo Yuan, Mario Szegedy, Yaoyun Shi, and Jianxin Chen. Classical simulation of quantum supremacy circuits, 2020.
- [29] Hsin-Yuan Huang, Richard Kueng, and John Preskill. Predicting many properties of a quantum system from very few measurements. *Nature Physics*, 16(10):1050–1057, 2020.
- [30] Yipeng Huang, Steven Holtzen, Todd Millstein, Guy Van den Broeck, and Margaret Martonosi. Logical abstractions for noisy variational quantum algorithm simulation. In *Proceedings of the 26th ACM International Conference on Architectural Support for Programming Languages and Operating Systems*, ASPLOS '21, page 456–472, New York, NY, USA, 2021. Association for Computing Machinery.
- [31] Yuwei Jin, Xiangyu Gao, Minghao Guo, Henry Chen, Fei Hua, Chi Zhang, and Eddy Z. Zhang. Quantum fourier transformation circuits compilation, 2023.
- [32] Yuwei Jin, Fei Hua, Yanhao Chen, Ari Hayes, Chi Zhang, and Eddy Z. Zhang. Exploiting the regular structure of modern quantum architectures for compiling and optimizing programs with permutable operators. In *Proceedings of the 28th ACM International Conference on Architectural Support for Programming Languages and Operating Systems, Volume 4*, ASPLOS '23, page 108–124, New York, NY, USA, 2024. Association for Computing Machinery.
- [33] Yuwei Jin, Zirui Li, Fei Hua, Tianyi Hao, Huiyang Zhou, Yipeng Huang, and Eddy Z. Zhang. Tetris: A compilation framework for vqa applications in quantum computing. In *2024 ACM/IEEE 51st Annual International Symposium on Computer Architecture (ISCA)*, pages 277–292, 2024.
- [34] Shuwen Kan, Zefan Du, Miguel Palma, Samuel A Stein, Chenxu Liu, Wenqi Wei, Juntao Chen, Ang Li, and Ying Mao. Scalable circuit cutting and scheduling in a resource-constrained and distributed quantum system, 2024.
- [35] Abhinav Kandala, Antonio Mezzacapo, Kristan Temme, Maika Takita, Markus Brink, Jerry M. Chow, and Jay M. Gambetta. Hardware-efficient variational quantum eigensolver for small molecules and quantum magnets. *Nature*, 549(7671):242–246, 2017.
- [36] Phillip Kaye, Raymond Laflamme, and Michele Mosca. *An Introduction to Quantum Computing*. Oxford University Press, Inc., USA, 2007.
- [37] Junpyo Kim, Dongmoon Min, Jungmin Cho, Hyeonseong Jeong, Ilkwon Byun, Junhyuk Choi, Juwon Hong, and Jangwoo Kim. A fault-tolerant million qubit-scale distributed quantum computer. In *Proceedings of the 29th ACM International Conference on Architectural Support for Programming Languages and Operating Systems, Volume 2*, ASPLOS '24, page 1–19, New York, NY, USA, 2024. Association for Computing Machinery.
- [38] Angelika Kimmig, Guy Van den Broeck, and Luc De Raedt. Algebraic model counting. *Journal of Applied Logic*, 22:46–62, 2017. SI:Uncertain Reasoning.
- [39] Daphne Koller and Nir Friedman. *Probabilistic Graphical Models: Principles and Techniques - Adaptive Computation and Machine Learning*. The MIT Press, 2009.
- [40] F.R. Kschischang, B.J. Frey, and H.-A. Loeliger. Factor graphs and the sum-product algorithm. *IEEE Transactions on Information Theory*, 47(2):498–519, 2001.
- [41] Nicholas LaRacuenta, Kaitlin N Smith, Poolad Imany, Kevin L Silverman, and Frederic T Chong. Modeling short-range microwave networks to scale superconducting quantum computation. *arXiv preprint arXiv:2201.08825*, 2022.
- [42] Gushu Li, Yunong Shi, and Ali Javadi-Abhari. Software-hardware co-optimization for computational chemistry on superconducting quantum processors. In *Proceedings of the 48th Annual International Symposium on Computer Architecture*, ISCA '21, page 832–845. IEEE Press, 2021.
- [43] Hao Li, Asim Kadav, Igor Durdanovic, Hanan Samet, and Hans Peter Graf. Pruning filters for efficient convnets. In *International Conference on Learning Representations*, 2017.
- [44] Igor L. Markov and Yaoyun Shi. Simulating quantum computation by contracting tensor networks. *SIAM Journal on Computing*, 38(3):963–981, 2008.
- [45] Sam McArdle, Suguru Endo, Alán Aspuru-Guzik, Simon C. Benjamin, and Xiao Yuan. Quantum computational chemistry. *Rev. Mod. Phys.*, 92:015003, Mar 2020.
- [46] N. David Mermin. *Quantum Computer Science: An Introduction*. Cambridge University Press, 2007.
- [47] Prakash Murali, Dripto M. Debroy, Kenneth R. Brown, and Margaret Martonosi. Architecting noisy intermediate-scale trapped ion quantum computers. In *Proceedings of the ACM/IEEE 47th Annual International Symposium on Computer Architecture*, ISCA '20, page 529–542. IEEE Press, 2020.
- [48] Engineering National Academies of Sciences, Medicine, Division on Engineering, Physical Sciences, Intelligence Community Studies Board, Computer Science, Telecommunications Board, Committee on Technical Assessment of the Feasibility, Implications of Quantum Computing, M. Horowitz, and E. Grumblng. *Quantum Computing: Progress and Prospects*. National Academies Press, 2019.
- [49] Michael A. Nielsen and Isaac L. Chuang. *Quantum Computation and Quantum Information: 10th Anniversary Edition*. Cambridge University Press, USA, 10th edition, 2011.
- [50] Aditya Pawar, Yingheng Li, Zewei Mo, Yanan Guo, Youtao Zhang, Xulong Tang, and Jun Yang. Integrated qubit reuse and circuit cutting for large quantum circuit evaluation, 2023.
- [51] Judea Pearl. *Probabilistic Reasoning in Intelligent Systems: Networks of Plausible Inference*. Morgan Kaufmann Publishers Inc., San Francisco, CA, USA, 1988.
- [52] Edwin Pednault, John A. Gunnels, Giacomo Nannicini, Lior Horesh, and Robert Wisnieff. Leveraging secondary storage to simulate deep 54-qubit sycamore circuits, 2019.
- [53] Tianyi Peng, Aram W. Harrow, Maris Ozols, and Xiaodi Wu. Simulating large quantum circuits on a small quantum computer. *Phys. Rev. Lett.*, 125:150504, Oct 2020.
- [54] Alberto Peruzzo, Jarrod McClean, Peter Shadbolt, Man-Hong Yung, Xiao-Qi Zhou, Peter J. Love, Alán Aspuru-Guzik, and Jeremy L. O'Brien. A variational eigenvalue solver on a photonic quantum processor. *Nature Communications*, 5(1):4213, 2014.
- [55] John Preskill. Quantum Computing in the NISQ era and beyond. *Quantum*, 2:79, August 2018.
- [56] Eleanor Rieffel and Wolfgang Polak. An introduction to quantum computing for non-physicists. *ACM Comput. Surv.*, 32(3):300–335, sep 2000.
- [57] Stuart Russell and Peter Norvig. *Artificial Intelligence: A Modern Approach*. Prentice Hall Press, USA, 3rd edition, 2009.
- [58] Kaitlin N. Smith, Michael A. Perlin, Pranav Gokhale, Paige Frederick, David Owusu-Antwi, Richard Rines, Victory Omole, and Frederic Chong. Clifford-based circuit cutting for quantum simulation. In *Proceedings of the 50th Annual International Symposium on Computer Architecture*, ISCA '23, New York, NY, USA, 2023. Association for Computing Machinery.

- [59] Wei Tang and Margaret Martonosi. Scaleqc: A scalable framework for hybrid computation on quantum and classical processors, 2022.
- [60] Wei Tang, Teague Tomesh, Martin Suchara, Jeffrey Larson, and Margaret Martonosi. Cutqc: Using small quantum computers for large quantum circuit evaluations. In *Proceedings of the 26th ACM International Conference on Architectural Support for Programming Languages and Operating Systems*, ASPLOS '21, page 473–486, New York, NY, USA, 2021. Association for Computing Machinery.
- [61] Hanrui Wang, Yongshan Ding, Jiaqi Gu, Yujun Lin, David Z. Pan, Frederic T. Chong, and Song Han. QuantumNAS: Noise-Adaptive Search for Robust Quantum Circuits . In *2022 IEEE International Symposium on High-Performance Computer Architecture (HPCA)*, pages 692–708, Los Alamitos, CA, USA, April 2022. IEEE Computer Society.
- [62] Hezi Zhang, Keyi Yin, Anbang Wu, Hassan Shapourian, Alireza Shabani, and Yufei Ding. Mech: Multi-entry communication highway for superconducting quantum chiplets. In *Proceedings of the 29th ACM International Conference on Architectural Support for Programming Languages and Operating Systems, Volume 2*, ASPLOS '24, page 699–714, New York, NY, USA, 2024. Association for Computing Machinery.